CHAPTER 2

Efficient Design of Curved Solar Air Heater Integrated with Semi-down Turbulators

Recent investigations reveal that curved solar air heaters (SAH) thermo-hydrodynamically performs better in comparison to flat SAH design. Further, it has been observed that down configurations of turbulators or extended surfaces on the flat plate solar collector significantly enhance the thermal performance. However, scientific literature on thermal performance investigations with down configurations of ribs in curved SAH are rare. In the chapter, we systematically investigate using experimentally validated computational fluid dynamics model for different shapes of downconfiguration of ribs. It was observed that half-trapezoidal and quarter-circular shape ribs shows maximum increase in thermal performance i.e. 17% and 16% , respectively, however frictional loss for quarter-circular ribs was observed to be less by about 10% when compared to trapezoidal shape ribs. The exergy recovery is maximum for trapezoidal and circular shape ribs and it is about 35% more than the smooth flat SAH. A new correlation has been developed for Nusselt number variation which has the form as $Nu = f\left[Re, \frac{e_r}{H}\right]$ where e_r is the height of quarter-circle groove. Observed data from the model matches well with the prediction from the developed correlation.

2.1 Introduction

Thermo-hydraulic efficiency of any device depends the flow passage design and how the fluid interacts with heated surfaces inside the passage. The efficiency of solar air heating device largely depends on the design of absorber plate and flow passage duct [25, 50]. This is the reason many investigators have focused their research on various aspect of SAH designs specifically the

absorber plate and the duct integrated with different shapes of ribs or tabulators such as circular [144] and square [21, 126, 146] transverse ribs, tapered rectangular sectioned [38], various arrangements of V-shape ribs [71, 78, 137], wavy delta winglets [19, 119, 135], anchor-shaped inserts [18], perforated winglet vortex generators and cylindrical inserts [20, 133] , saw-tooth ribs [72] and many more such designs. With increasing cost of energy generation by using non-renewable fuel resources such as coal, crude oil, etc., and due to their limited stock and non-renewable nature, developing efficient designs of devices that use renewable sources such as solar energy has become imperative [36] . Since flat plate SAH is used widely in many domestic and industrial applications such as room heating, agricultural crop drying, desalination, and other heating applications, improving the designs for better thermal performance would significantly contribute to our growing energy needs. Furthermore, since the availability of average peak sunlight hours is only about 4 to 6 hours/day, in this short duration the SAH must be thermally efficient to avail maximum portion of the available solar energy.

There are two important aspects of SAH design: absorber plate and the flow duct where cold air enter, gains the energy from the heated plate and exits the passage [28]. Most of the previous studies on SAH performance have been conducted in a flat duct [4, 35, 85] . However, few recent investigations [87, 123, 124]have shown that curved SAH performs better compared to flat SAH design. Secondary flows near the curved surfaces enhance heat transfer [123, 124] . The other aspect of SAH design is the absorber plate over which ribs or tabulators are integrated to improve thermal performance. Depending on the configuration of SAH, the absorber plate is either placed on the top i.e. down-configuration [38, 71, 72, 78, 144, 146](see Fig. 2.1(a)) or bottom i.e. up-configuration [7, 21, 64, 119, 135, 137](see Fig. 2.1(b)) of the flat duct. The investigations show that though the interaction of cold fluid with heated flat absorber plate increases with addition of tabulators in either position, down-configuration of ribs shows the higher mean temperature of air as compared to ribs in the up arrangement [72]. The secondary flows[102] mix with the main air flowing between the discrete ribs after traveling little distance which leads to an enhanced mixing rate of secondary flow with the main flow near the absorber plate. However, there is always some compromise between thermal and hydraulic performance. The additional gain in thermal performance achieves by imparting more turbulence in the flow which consequently increases the hydraulic losses.

As mentioned above, curved designs of solar air heater duct [87, 123–125] show considerable enhancement in the thermal characteristics when compared to flat plate SAH design with the former showing minor drop in hydraulic performance. Due to centrifugal effect, curved SAH exhibit the formation of secondary vortices resulting in the mixing flow [102, 123]. Further, formation of dean vortices enhances the heat transfer rate in curved SAH [87] . These effects are absent in flat plate SAH. However, there are still many open scientific issues that need to be addresses vis-à-vis curved SAH thermal performance. For example, effect of integrating down-configuration ribs on the curved SAH absorber plate has not yet been investigated. Further, as

literature points out, the shape of ribs plays a significant role in SAH performance. The effect of integrating various shapes of down-configuration ribs with curved SAH is yet to be understood properly. From the above discussion, it is clear that studies on curved SAH equipped with down-configuration ribs are scarce which motivated the authors to conduct the present analysis to investigate the best rib designs for higher thermo-hydraulic performance.

In this chapter, we have addressed these issues in a systematic manner using an experimentally validated numerical model for a wide range of geometrical parameters of the roughened geometry in a curved SAH. Further, a suitable correlation has been developed for Nusselt number variation as function of Reynolds number and geometrical parameters for the best design of turbulator. It was observed that the down-configuration half-trapezoidal and quarter-circle ribs in curved SAH show higher thermal performance. A new correlation has been developed for Nusselt number variation as a function of relative quarter-circle groove height ratio that predicts thermal performance for a wide range of Reynolds numbers. Authors hope that the investigations presented in the chapter would be beneficial to the scientific community in further designing thermally efficient designs of solar air heaters.

2.2 Numerical domain

Geometric details, mesh generation, boundary conditions, and grid independence study are described in the subsequent sub-sections.

2.2.1 Geometry specification and parametric details

The flow domain of flat and curved (25°curvature angle) SAH, comprises of rectangular cross-sectional shape flow passage through which fluid medium flows. The flow passage has an inlet section at one end to allow fluid medium to enter into flow channel and an outlet section at the other end for the exit. The geometrical dimensions of SAH are described in terms of length and opening height of the duct which are taken as 1600 mm and 40 mm, respectively, such that surface area of both flat and curved SAH are identical as shown in Fig. 2.1. The best curvature angle 25°[125] having a radius of curvature of 3647 mm is identical for all the curved SAH models. The designs of different shapes of ribs considered in the present study are (i) half-triangular, (ii) half-trapezoidal and (iii) quarter-circle, see Fig. 2.2.

The geometrical parameters of various shape of ribs are: (i) e_t and b_t are the height and width of half-triangular groove, which are equal for the case of isosceles triangle; (ii) e_{tp}, b_{tp} and b_{tpd} are the height, width of top and bottom of half-trapezoidal groove; and (iii) e_r and b_r are the height and width of quarter-circle groove.

The numerical domain of SAH has an air inlet and outlet section, a top metallic absorber plate to absorb a maximum portion of incident solar radiation and rest surfaces are kept as

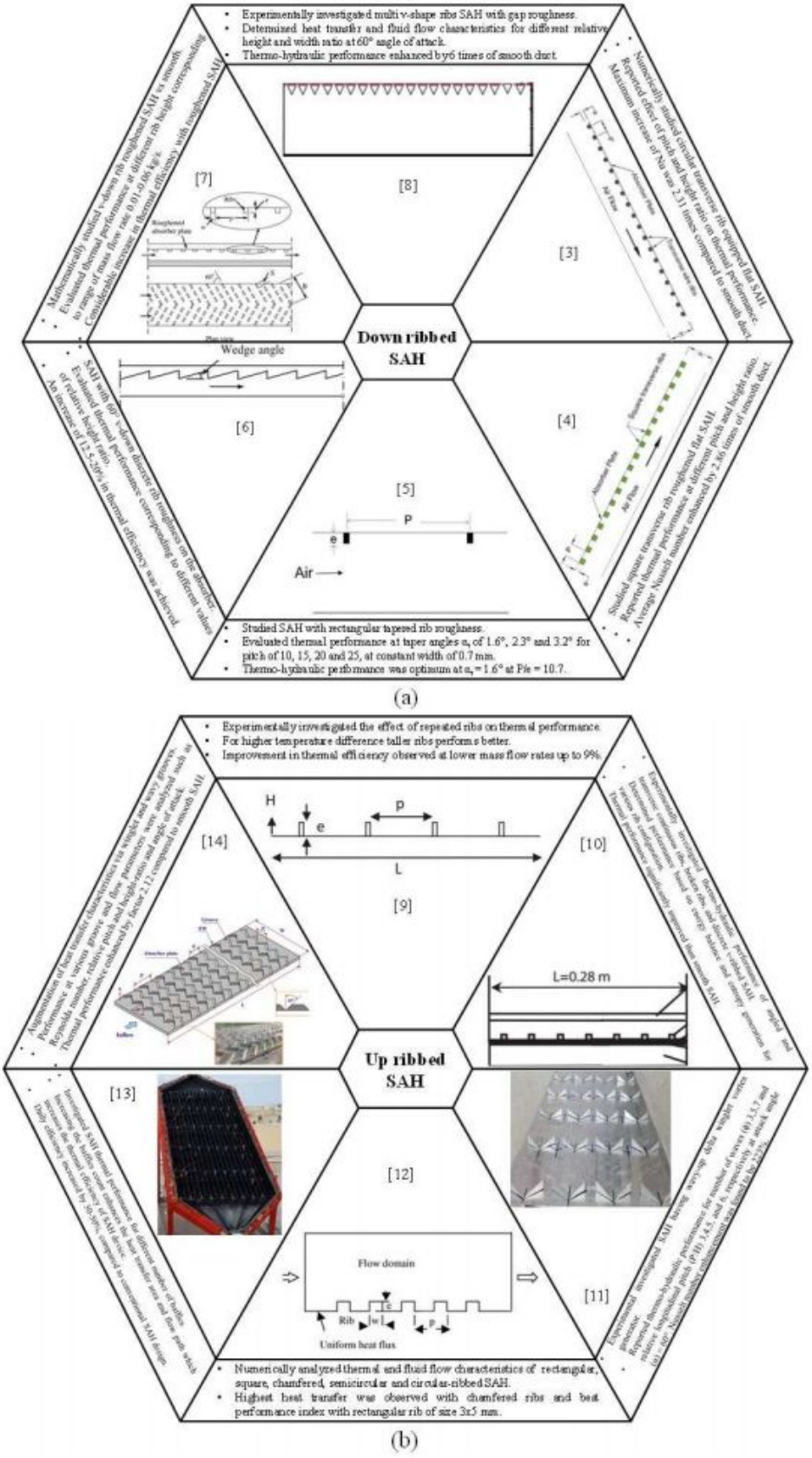

Figure 2.1: Previous investigations based on solar air heater straight flow channel equipped with various shape of ribs in two different arrangements of ribbed absorber plate: (a) down ribs and (b) up/bottom ribs.

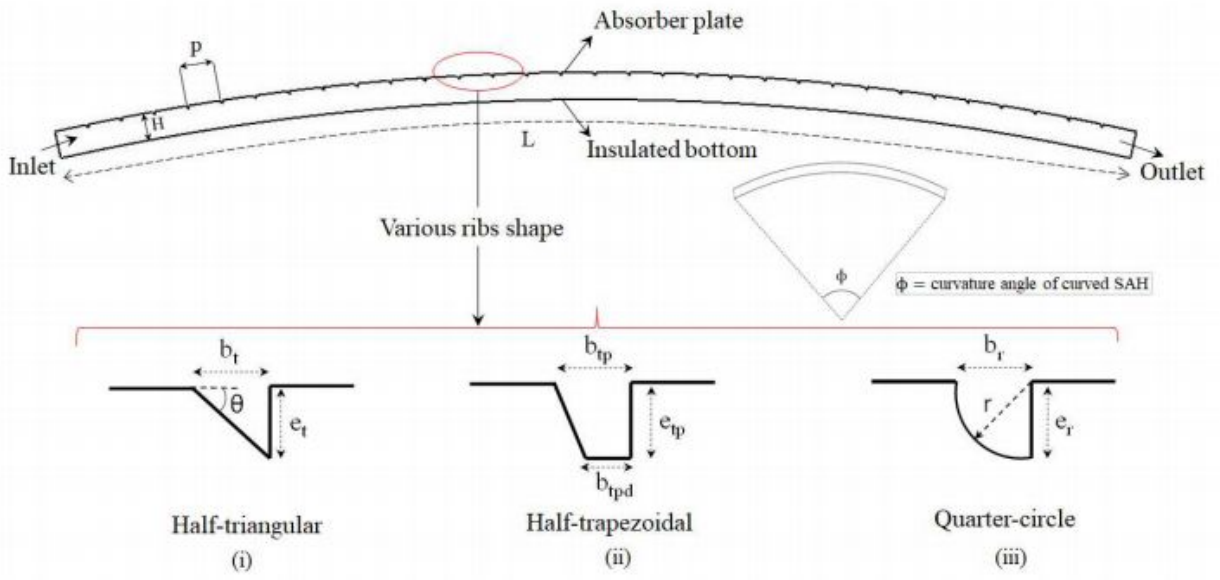

Figure 2.2: Geometry of a curved SAH having 25° curvature angle with the half-triangular (i.e. (i)) grooved absorber plate. The three different shape of ribs have been considered in the study are shown: (i) half-triangular, (ii) half-trapezoidal and (iii) quarter-circle, and analyzed individually to investigate thermo-hydraulic performance.

adiabatic (ensures no thermal interaction with the ambient condition) [4, 123]. A fixed value of heat flux (q) has been assigned to the absorber plate. Air i.e. fluid medium at a specific velocity corresponding to a particular value of Reynolds number (Re) enters from the inlet section of the flow channel where it interacts with the hot absorber surface which rises fluid temperature and finally exit from the outlet section. The cases considered in the present study have been simulated numerically for the range of Re 11000 – 15000. The design and flow parameters are mentioned below in Table 2.1.

2.2.2 Mesh description and grid independence of numerical model

The finite volume method (FVM) was used to discretize the computational domain. A two-dimensional flow domain has been meshed using unstructured tria shape elements to analyze the hydraulic and thermal characteristics of the flow domain. Very fine mesh region near the ribs has been generated using very small size element for better observation of flow characteristics and thermal behavior of the device (see Fig. 2.3). The swirl motion generated at high speed flows near the ribbed absorber plate were more closely captured by fine mesh region. Near wall dimensionless distance y^+ was kept at less than unity. The modeling and simulation analysis has been conducted using Altair HyperWorks and STAR-CCM+ software.

A grid independence study has been conducted to make certain that results are independent of grid sizes used in the model. The selection of optimum grid size has been determined after performing the grid independence test for flat conventional SAH geometry. The variation in the

Table 2.1: Description of design and flow parameters.

S. No.	Parameters	Values/range
1	Relative half-triangular, half-trapezoidal and quarter-circular-groove height ratio (e_t/H, e_{tp}/H and e_r/H)	• $e_t/H = 0.125$ • $e_{tp}/H = 0.125$ • $e_r/H = 0.125$
2	Relative rib height to width ratio (e_t/b_t, e_{tp}/b_{tp} and e_r/b_r)	• $e_t/b_t = 0.267, 0.466, 0.7, 1$ $b_t = 5$ mm • e_{tp}/b_{tp}=1, Parallel sides of half-trapezoidal rib are b_{tp}=5 mm & b_{tpd}=3 mm
3	Pitch (P)	P = 50 mm (fixed)
4	Reynolds number (Re)	11000 – 15000

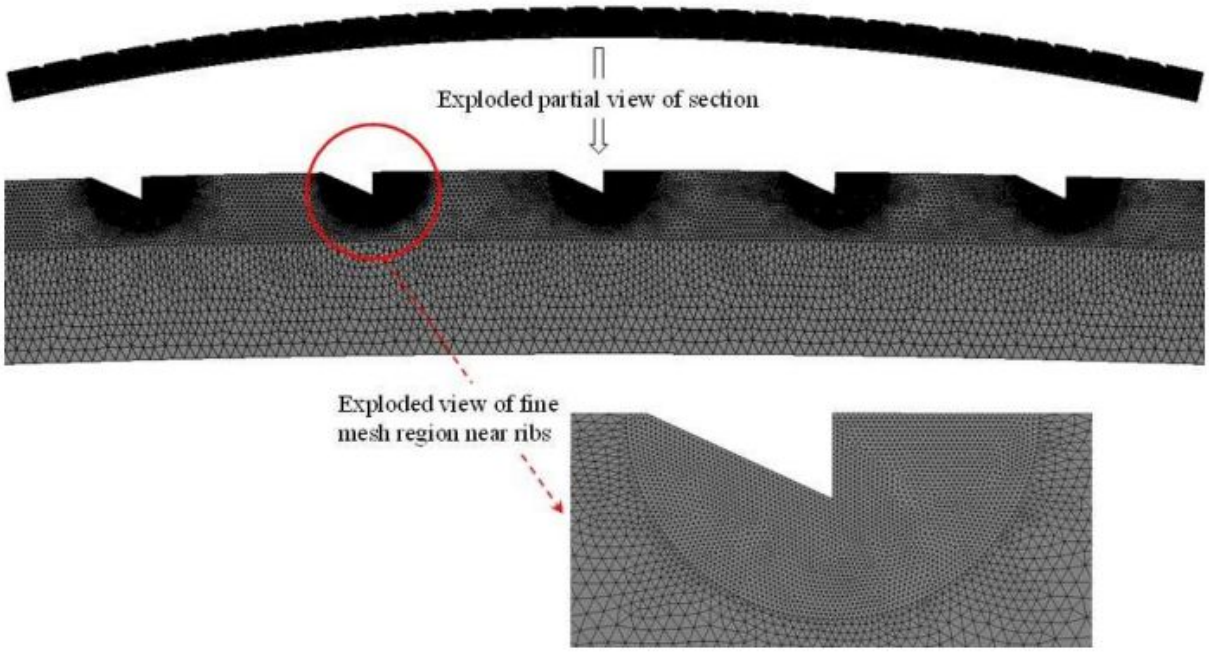

Figure 2.3: Mesh of the computational flow domain of curved SAH equipped with half-triangular shape ribs.

Table 2.2: Grid independence test.

S. No.	Element counts	ΔT_o (in %)	ΔNu (in %)
1	228304	-	-
2	179648	0.00047	0.454
3	146156	0.00098	0.5
4	121056	0.00028	0.51
5	99920	0.0064	2.29

Table 2.3: Air properties at 300 K.

Properties name	Value
Absolute viscosity (μ)	1.855 x 10-5 Ns/m^2
Thermal conductivity (k)	0.026 W/m K
Prandtl number (Pr)	0.71
Specific heat (C_P)	1003.62 J/kg K
Density (ρ)	1.184 kg/m^3

parameters has been recorded in the form of temperature of air at the outlet section (T_o) and Nusselt number (Nu) against different numbers of cells. The Nusselt number values have been calculated based on the hydraulic diameter of the cross-section corresponding to the unit depth of the SAH duct i.e. D_e= 0.076 m. The parametric variations in percentage have been noted with respect to element counts under identical sets of boundary conditions. The number of element counts varied from 228304 to 179648, 179648 to 146156, 146156 to 121056 and 121056 to 99920 and corresponding change in T_o values are 0.00047% , 0.00098% , 0.00028% and 0.0064% ; and for Nu are 0.454% , 0.5% , 0.51% and 2.29%, respectively, as shown in Table 2.2. The small variations in results indicate that the initial element count was near the optimum value. The number of elements 146156 has been selected as optimum due to insignificant variation in the parametric values.

2.2.3 Boundary conditions

All the considered cases were simulated under a fixed value of absorber heat flux, $q = 1000\,W/m^2$[4, 144]. The flow velocity value has been assigned corresponding to particular Reynolds number, Re. The atmospheric condition was maintained at the outlet section by assigning gauge pressure value equals to zero (i.e. atmospheric condition), and rest walls were assumed as adiabatic (i.e. assuming no heat loss to ambient). The walls are subjected to no-slip boundary condition. Each case has been simulated for the range of Re 11000 – 15000. The flow has been considered as an incompressible flow assuming fluid density to be independent of change in the pressure values. The air behaves more closely to an ideal gas at STP (standard temperature and pressure) and hence treated as an ideal gas. The air properties are mentioned below in Table 2.3.

2.2.4 Governing equations and physical terms

The two-dimensional flow domain has been exposed to boundary conditions explained in the above sub-section 2.3 in order to solve equations of mass conservation, momentum and energy of the flow domain[36]. The semi-implicit method for pressure linked equations (SIMPLE) algorithm has been adopted to resolve the velocity and pressure of the flow field. The basic governing equations i.e. continuity, momentum, and energy equations were solved for incompressible flow under steady-state condition using the second-order upwind scheme. The numerical data obtained for different cases have been recorded when the constraint for the convergence i.e. $10^{-5}$for mass conservation equation and $10^{-3}$for energy equation were achieved[15, 16] . Under the above mentioned criterion, the parametric variation becomes insensitive to successive iterations.

Continuity equation,

$$\frac{\partial u}{\partial x}+\frac{\partial v}{\partial y}=0 \tag{2.1}$$

Momentum equations,

$$\rho\left[\frac{\partial(uu)}{\partial x}+\frac{\partial(uv)}{\partial y}\right]=-\frac{\partial p}{\partial x}+\frac{\partial}{\partial x}\left[(\mu+\mu_t)\frac{\partial u}{\partial x}\right]+\frac{\partial}{\partial y}\left[(\mu+\mu_t)\frac{\partial u}{\partial y}\right]-\frac{2}{3}\rho\frac{\partial k}{\partial x} \tag{2.2}$$

$$\rho\left[\frac{\partial(uv)}{\partial x}+\frac{\partial(vv)}{\partial y}\right]=-\frac{\partial p}{\partial y}+\frac{\partial}{\partial x}\left[(\mu+\mu_t)\frac{\partial v}{\partial x}\right]+\frac{\partial}{\partial y}\left[(\mu+\mu_t)\frac{\partial v}{\partial y}\right]-\frac{2}{3}\rho\frac{\partial k}{\partial y}-\rho g \tag{2.3}$$

Energy equation,

$$\rho\left[\frac{\partial(uT)}{\partial x}+\frac{\partial(vT)}{\partial y}\right]=\frac{\partial}{\partial x}\left[\left(\frac{K}{C_P}+\frac{\mu_t}{Pr_t}\right)\frac{\partial T}{\partial x}\right]+\frac{\partial}{\partial y}\left[\left(\frac{K}{C_P}+\frac{\mu_t}{Pr_t}\right)\frac{\partial T}{\partial y}\right] \tag{2.4}$$

where and $Pr_t$is the turbulent Prandtl number, k denote turbulent kinetic energy, and μ_t denote turbulent viscosity. The other two turbulent kinetic and dissipation equations are:

$$\nabla\cdot\left(\rho k\overline{V}\right)=\nabla\cdot\left[\left(\mu+\frac{\mu_t}{\sigma_k}\right)\nabla k\right]+G_k+G_b-\rho\varepsilon-\gamma_M+S_k \tag{2.5}$$

$$\nabla\cdot\left(\rho\varepsilon\overline{V}\right)=\nabla\cdot\left[\left(\mu+\frac{\mu_t}{\sigma_\varepsilon}\right)\nabla\varepsilon\right]+C_{\varepsilon1}\frac{\varepsilon}{k}(G_k+C_{\varepsilon3}G_b)-C_{\varepsilon2}\rho\frac{\varepsilon^2}{k}-R_\varepsilon+S_\varepsilon \tag{2.6}$$

G_k and G_b denotes turbulent production and buoyancy production, respectively.

The values of parameters σ_T , σ_k , and σ_ε are 1.0, 1.0, and 1.2, respectively, whereas turbulence model constants i.e. $C_{\varepsilon1}$ =1.44, $C_{\varepsilon2}$ =1.9 and C_μ =0.09, where $Pr_t = 0.9$.

Reynolds number denotes the ratio of inertia force to the viscous force, and its major significance to differentiate among laminar and turbulent flow.

$$Re = \frac{\text{Inertia force}}{\text{Viscous force}} = \frac{\rho v D_e}{\mu} \tag{2.7}$$

Where $D_e = \frac{4A}{P}$, A is the cross-sectional area of the duct and P is the wetted perimeter.

Dean number has significance to predict flow behavior in a curved flow channels under laminar and turbulent flow conditions.

$$D_n = Re\sqrt{\frac{D_H}{R_C}} \tag{2.8}$$

where, $D_H = 0.5H$, and H is the opening height of the SAH duct.

The considered range of Re and D_n are 11000-15000 and 1587-2165, respectively which falls under a fully turbulent flow region, and therefore entire study has been simulated by considering the flow under fully turbulent region.

The thermo-hydraulic characteristic of SAH has been determined in terms of temperature factor $\frac{(T_o - T_i)}{I}$, Nusselt number Nu, friction factor f, turbulent dissipation rate, and vorticity magnitude. The temperature factor represents rise in temperature of air at outlet of SAH with respect to ambient temperature per unit solar radiant energy received by the collector, higher value indicates higher thermal effectiveness of the device.

$$Temperature\,factor = \frac{(T_o - T_i)}{I} \tag{2.9}$$

Friction factor is determined from pressure drop, ΔP that occurs as a result of resistance to flow along the flow channel can be obtained as,

$$f = \frac{\Delta P D_e}{2\rho L V^2} \tag{2.10}$$

where D_e denote the equivalent diameter of the flow channel cross-section, mm; v is the flow velocity, m/s.

Nusselt number indicates the rate of heat exchange from the hot absorber plate to fluid medium can be evaluated as[79]

$$Nu = \frac{h\,D_e}{k} \tag{2.11}$$

where h is the convection heat transfer coefficient (W/m^2K)

The turbulent dissipation rate (ε) tells about the rate of turbulent energy absorbed to breakdown the large eddies up to the time when it fully transformed into heat energy due to viscous nature of the fluid or in other words it signifies that the conversion rate of turbulent kinetic energy into internal thermal energy. The formation of flow vortices in the flow vicinity enhances mixing rate which increases the rate of heat transfer.

$$\varepsilon = C_{\mu}^{3/4} \frac{k^{3/2}}{l} \tag{2.12}$$

Where $k = \frac{1}{2}\left(u'^2 + v'^2\right)$, is the turbulent kinetic energy, l is the length scale representative of the large-scale turbulence, C_{μ} is the dimensionless constant = 0.09.

2.2.5 Assessment of magnitude of solar radiation received on curved SAH

The magnitude of the solar radiation received by the curved SAH having moderate curvature angles is identical to the conventional flat plate SAH, and has been shown in the literatures[87, 123–125]. Hence, the globally received solar radiations on the slightly curved surface having small curvature angles would be unchanged has been experimentally shown[87] . Therefore, the absorber plate of curved and flat SAH have been exposed to identical heat flux for further investigations.

2.3 Experimental validation of numerical model of curved SAH

The numerical model of curved SAH was validated with the experimental data of curved SAH[87]. The computational domain has the same dimensions of the reported experimental setup. The flow has been considered to be steady and density variation was modeled as a function of temperature. To include the effect of radiation heat transfer, the top glass cover was assigned heat transfer coefficient using equation $h = 5.7 + 3.8V_{\infty}$ (W/m^2·K)[125, 136, 140], which gives $h = 17.1$ W/m^{2}K for the specific wind speed. Rest surfaces of the SAH were kept as adiabatic in the analysis. The numerical results of outlet air temperatures were recorded for the identical mass flow rates i.e. $m = 0.0172, 0.029\ and\ 0.0472$ kg/s.m^{2}which were considered in the literature[87]. Figure 2.4 shows the variation in predicted temperature with the experimental data for different range of heat flux for $m = 0.0172$ kg/s.m^2. Figures for other mass flow rates has not been shown. The percentage error in the outlet air temperature was calculated based on the relative error using the following formula:

$$Relative\,error = \frac{(T_o - T_i)_{numerical} - (T_o - T_i)_{experimental}}{(T_o - T_i)_{experimental}} \tag{2.13}$$

The relative error observed to be in the range 1.1-10.1% for $m = 0.0172$ kg/s.m^2, 0.5-1.4% for $m = 0.029$ kg/s.m^2 and 6.2 – 11% for $m = 0.0472$ kg/s.m^2 and heat flux range 800 – 1100 W/m^2. Since the errors are within the acceptable limit, the numerical model is thus validated and mimics experimental conditions. Four different turbulence models were considered: K-Epsilon, K-Omega, Reynolds-Stress and Spalart-Allmaras turbulence model, among which results obtained using K-Epsilon model were closely following the experimental data[87]. For the sake of brevity,

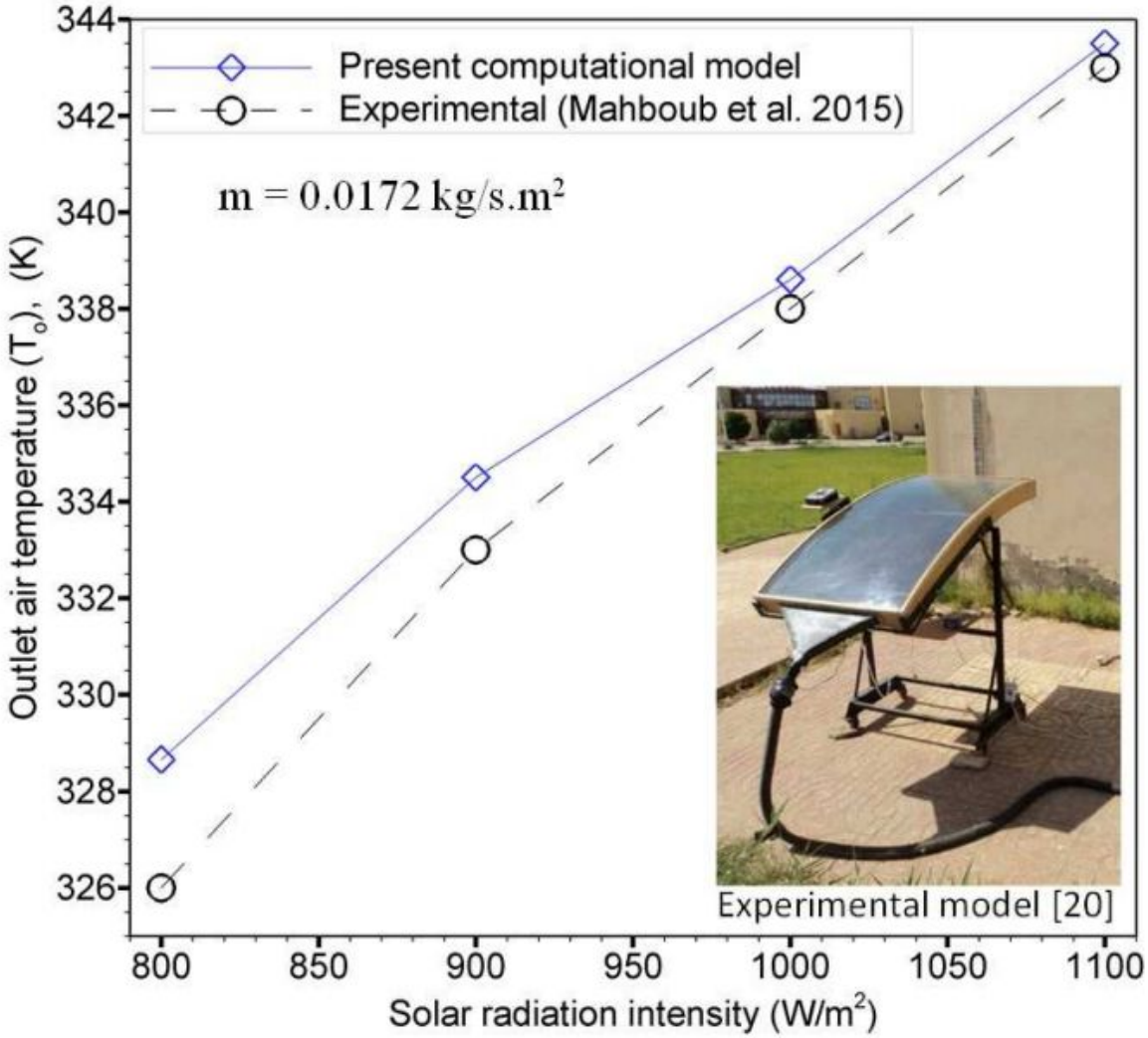

Figure 2.4: Outlet air temperature variation (T_o) with solar radiation intensity (I) at the mass flow rate of 0.0172 kg/s.m^2.

results from these turbulence models has not been presented here. Interested readers can refer to the recent literature[123] by the authors in which the effect of these turbulence models has been discussed.

2.4 Results and discussions

The variation of energy conversion and flow characteristics of different ribs integrated curved and flat SAH device have been carried out in this section. The variation of the flow and thermal characteristics have been determined in terms of Nusselt number, effectiveness, exergy, second law efficiency and friction losses, for the range of Reynolds number 11000 – 15000. The absorber plate was set to a constant heat flux of 1000 W/m^2. The ribs of the absorber plate intensifies turbulence in the flow, result of which more mixing in the flow increases the heat transfer rate at

the expense of pressure drop. In case of curved SAH, centrifugal and centripetal forces provides scope for the formation of dean/secondary flow vortices which has vortex pair of equal magnitude with opposite direction of rotation, one in clockwise and other in anti-clockwise. The curvature type flow channel augment the rate of heat exchange in the flow while interacting with the hot absorber plate.

The forces arises due to centrifugal action are strong enough to disturb the main flow velocity profile, which raises the rate of generation of secondary flow vortices near walls of the absorber surface as shown in Fig. 2.7. Due to centrifugal force flow has tendency to shift upward possess higher velocity compared to flat SAH (see Fig. 2.7).The dimensionless Dean number increases with increase in the Reynolds number values, which consequently raise the magnitude of centrifugal action/forces thereby manifesting in the form of high velocity variation near absorber walls in curved SAH compared to conventional flat SAH (see Fig. 2.7). The pressure drop values for the curved SAH has been seen to be slightly greater than the flat SAH due to curvature geometry of the flow channel.

Figure 2.5 shows the variation of temperature factor, $\frac{(T_o - T_i)}{I}$, for different shape of ribs for the range of Reynolds number 11000-15000, at $q = 1000\ \mathrm{W/m^2}$. The temperature factor represents the rise in temperature per unit solar insolation received by the SAH device[87]. The value of temperature factor decreases with increasing values of Reynolds number, as the flow velocity increases the interaction time duration of the flow with the hot absorber surface decreases. The maximum percentage increase in temperature factor in curved SAH over conventional flat SAH for trapezoidal ribs is 16.67% and it is 13.34% for quarter-circle ribs.

Figure 2.6 shows the variation of Nusselt number for different shape of ribs for *Re* in the range $11000 - 15000$, at $q = 1000\ \mathrm{W/m^2}$. The *Nu* values increases with increasing value of *Re*. The Nusselt number signifies the dominance of convection heat transfer over conduction heat transfer occurring from the absorber plate to flowing fluid. The values were found to be maximum for curved SAH compare to conventional flat SAH. The *Nu* values was found to be maximum for the triangular shape ribs having e_t/b_t=1 and e_t/H=0.125, which is 25.21% higher than the conventional flat SAH, whereas it is 22.56% higher for half-trapezoidal e_{tp}/b_{tp}=1 (parallel sides 5& 3 mm) and 19.28% for quarter-circle ribs e_r/b_r=1 (e_r=5 mm and b_r=5 mm). The height of the rib considerably effect the thermal performance of SAH device. The thermal performance has been improved with increase in the rib height for constant width. Enhanced thermal enactment has been attained due to generation of more turbulence which intensifies mixing in the flow. One interesting observation to be noted: Nusselt number in triangular ribs show marginally higher (about 2%) than trapezoidal ribbed SAH. One reason for this is that local velocity magnitude near the triangular ribs is slightly higher due to sharp pointed conical shape. Its cumulative effect is marginally higher heat transfer coefficient. It is then natural to expect higher air temperature at the outlet. However, result is observed contrary to it i.e. slightly lower outlet temperature than trapezoidal design ribs (see Fig. 2.5). One reason for this is that larger size vortices formed

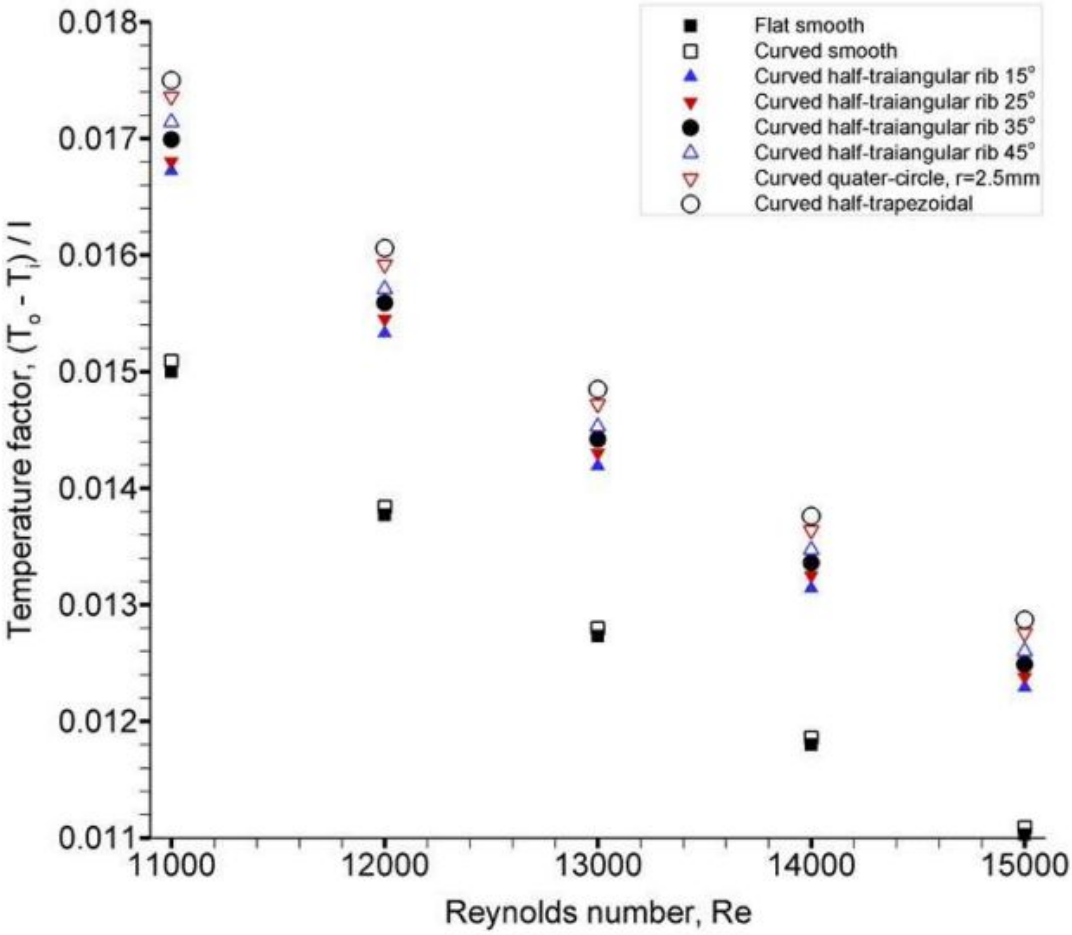

Figure 2.5: Variation of temperature factor, $\frac{(T_o - T_i)}{I}$, of curved SAH equipped with different shape of ribs for *Re* in the range 11000-15000, at $q = 1000\ \mathrm{W/m^2}$.

in triangular ribs do not dynamically attached and mix with the main stream as much as in trapezoidal ribs. Hence, heat transfer from vortices in triangular ribs mainly occurs through diffusion while convection heat transfer dominates near vortices in trapezoidal ribs due to better interaction and mixing with the main stream.

Figure 2.8 shows the friction factor variation of various shapes of ribs for *Re* in the range $11000 - 15000$, at $q = 1000\ \mathrm{W/m^2}$. Among three different ribs design for same height, the triangular ribs offer maximum obstruction to the upcoming flow in the flow channel and least obstruction for the quarter-circle ribs. In triangular ribs, the higher frictional losses occur due to sharp pointed tip; however, in quarter-circle ribs, less recirculating vortices are observed in the downstream. Similarly, in case of trapezoidal ribs, since the bottom edge is flat, less recirculation zone was observed than the triangular shaped ribs (see Figs. 2.14).

Thermally better designs are associated with higher pressure drop as half-triangular shape ribs having $e_t/b_t = 0.267$ and $e_t/H = 0.125$ associated with minimum frictional losses and hence has lowest thermal performance (see Fig. 2.5). However, by incorporating efficient ribs design,

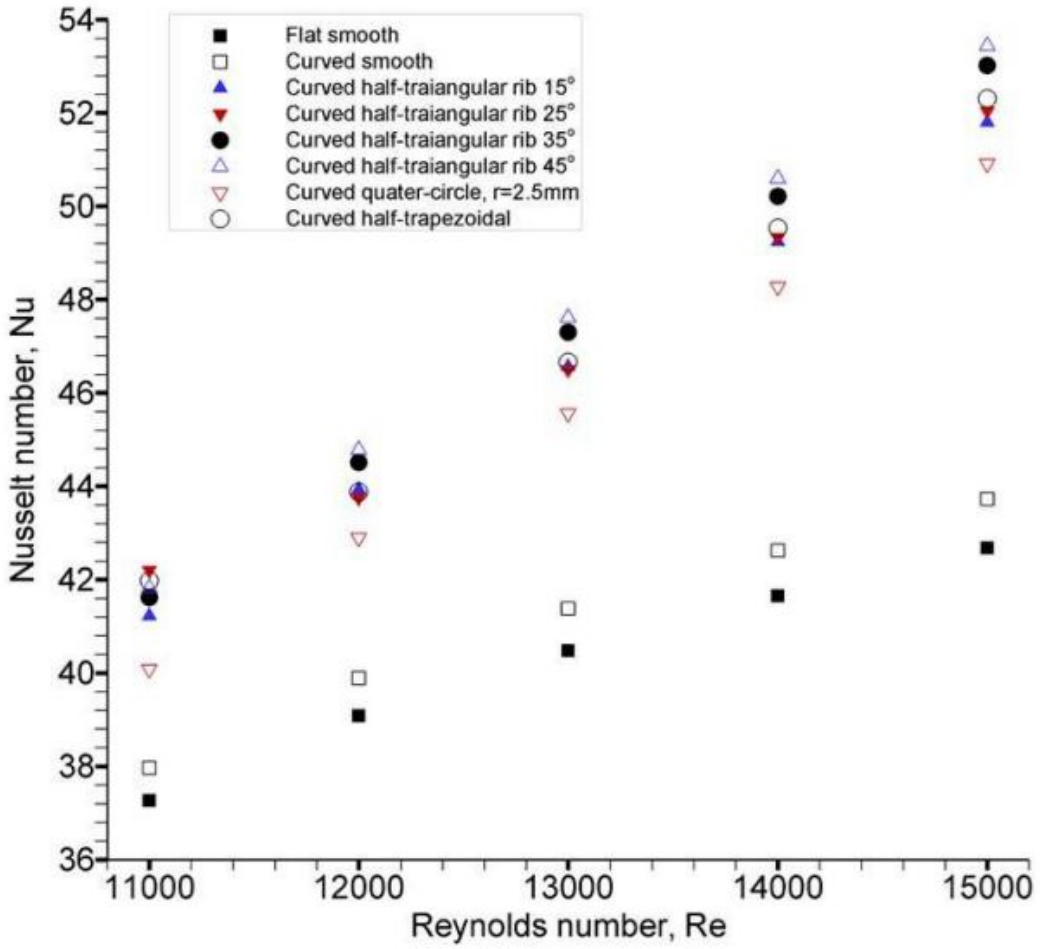

Figure 2.6: Shows Nusselt number variation for different shapes of ribs for Re in the range $11000-15000$, at $q = 1000\,\mathrm{W/m^2}$.

i.e. quarter-circle and half-trapezoidal, the device can achieve maximum thermal performance, keeping friction losses at moderate level. Among all, the SAH performs thermally higher for trapezoidal and quarter-circle shape ribs (see Fig. 2.5). However, in between these two best design, the quarter-circle ribs offer 10-12% higher thermo-hydraulic performance i.e. $\frac{(T_o-T_i)}{I}/f$, and Nusselt number per unit pressure drop ($Nu/\Delta P$) in comparison to half trapezoidal ribs see Fig. 2.9 and Fig. 2.10. The friction factor for half trapezoidal ribs has been found 7.78-9.64% higher than the quarter-circle ribs, for Re in the range $11000-15000$. Due to less hydraulic losses incurred and high thermal performance, the quarter-circle ribs design proven to be best among all different ribs design considered in the study.

The term thermal effectiveness can be defined as the ratio of actual temperature gradient between outlet air and ambient temperature to the maximum temperature gradient between absorber plate temperature and ambient temperature.

$$\varepsilon = \left(\frac{T_o - T_i}{T_s - T_i}\right) \tag{2.14}$$

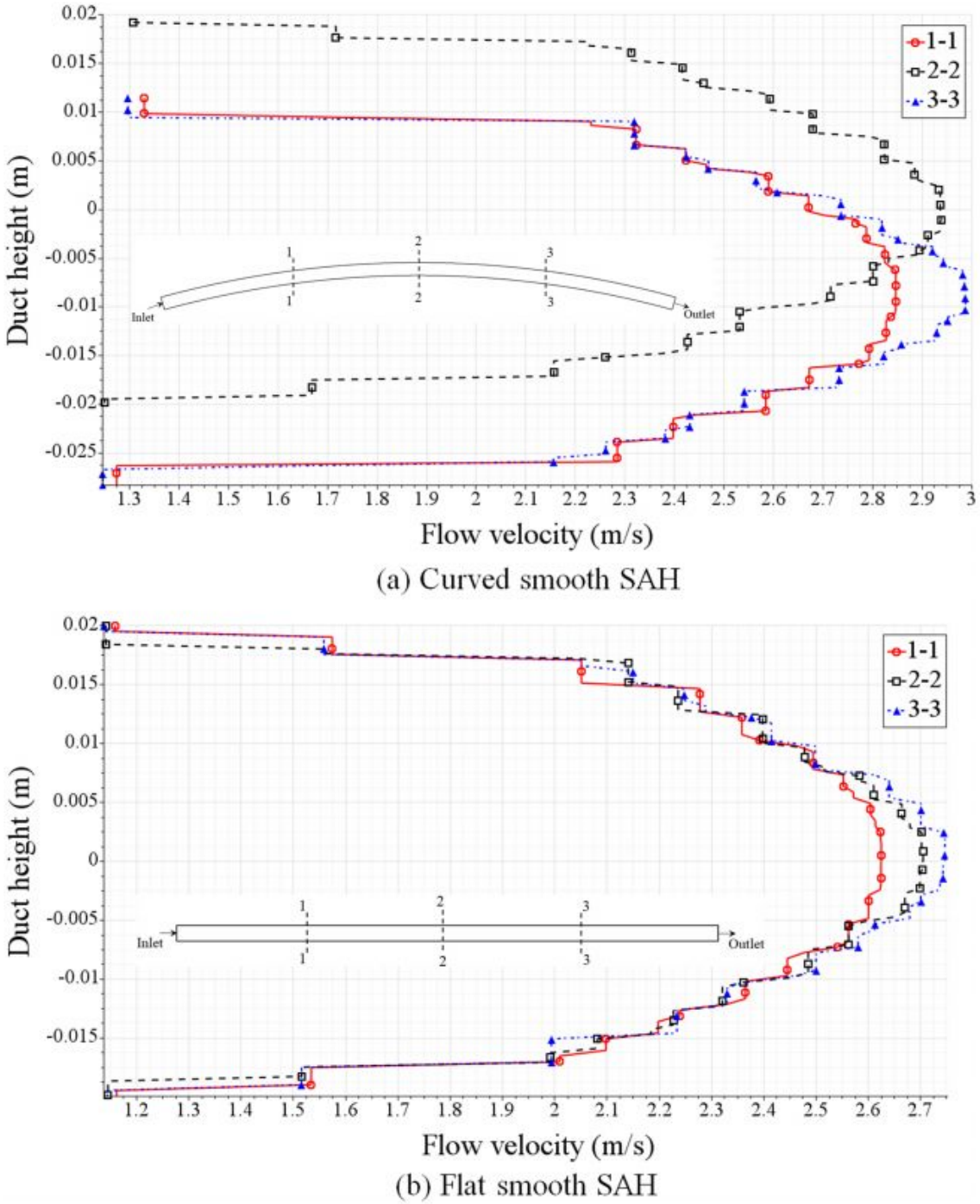

Figure 2.7: Flow velocity profiles of (a) curved smooth SAH and (b) flat smooth SAH at different axial locations along the duct height for Re in the range 11000 at $q = 1000\,\mathrm{W/m^2}$.

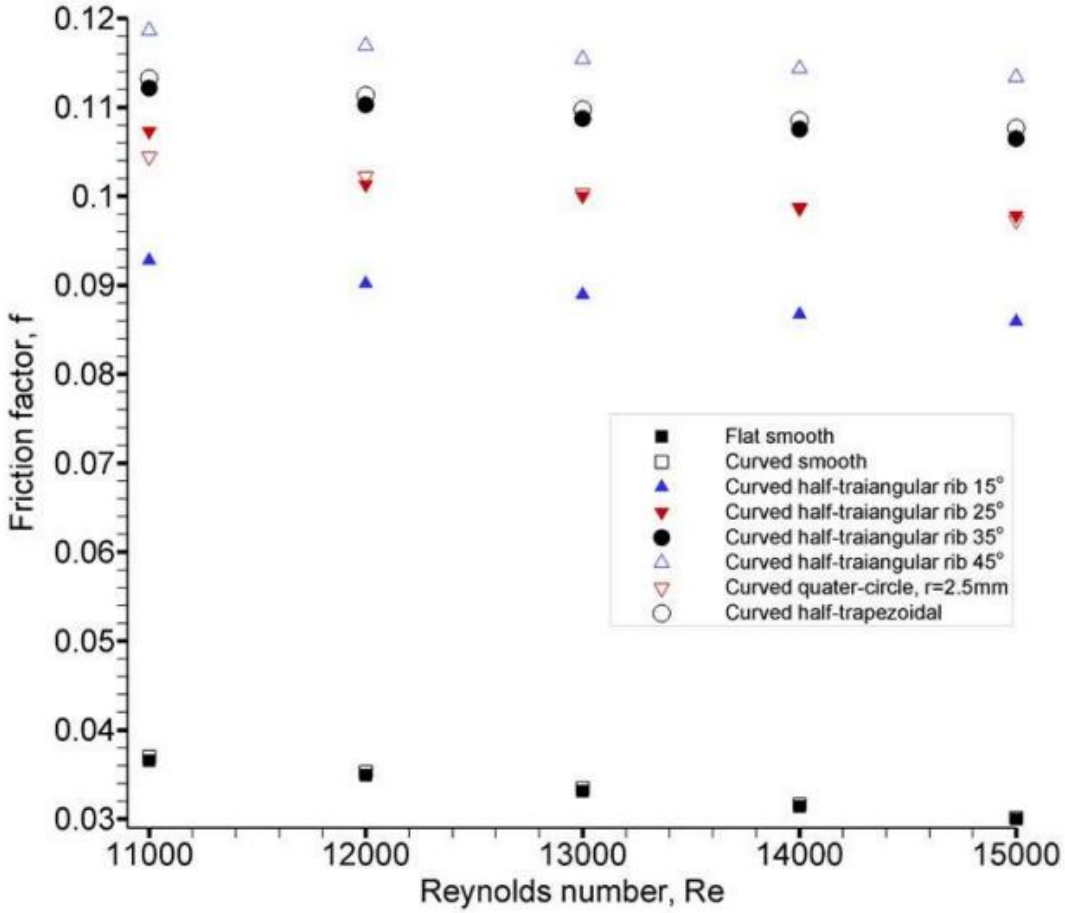

Figure 2.8: Friction factor variation for various shape of ribs for Re in the range 11000 – 15000, at $q = 1000$ W/m^2.

Figure 2.11 shows the variation of effectiveness of different shape of ribs with *Re* at $q = 1000$ W/m^2. The effectiveness denotes the thermal performance of the system. Among all ribs design, the half-trapezoidal shape ribs possess highest value and lowest was found for half-triangular shape ribs having $e_t/b_t = 0.267$ and $e_t/H = 0.125$.

2.5 Exergy analysis

Exergy analysis helps in designing energy efficient solar air heaters and facilitates in comparing various designs that are better suited for energy conversion[39] .

Now, mass, energy and exergy rate balance can be written in the following form:

$$\sum \dot{m}_{in} = \sum \dot{m}_{out} \tag{2.15}$$

$$\sum \dot{E}_{in} = \sum \dot{E}_{out} \tag{2.16}$$

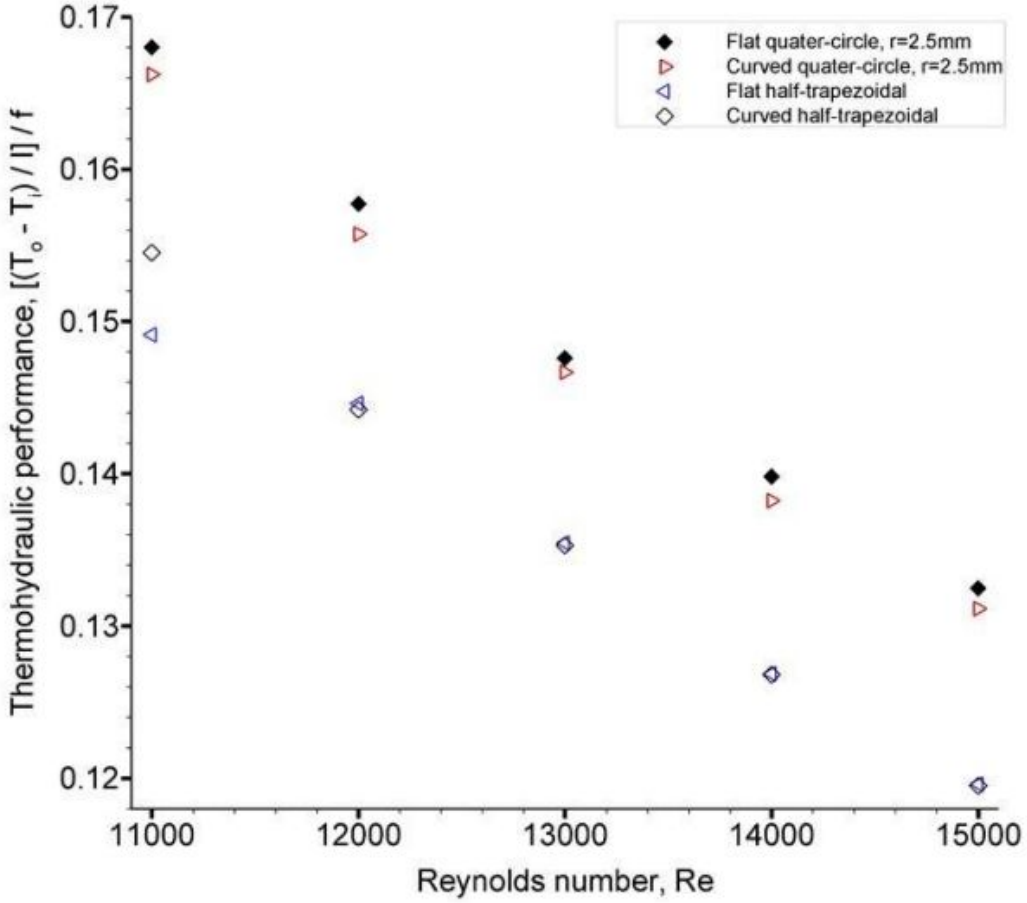

Figure 2.9: Thermohydraulic performance $\frac{(T_o - T_i)}{I} / f$, variation of different shape of ribs for Re in the range $11000 - 15000$, at $q = 1000\ \mathrm{W/m^2}$.

$$\sum \dot{E}_{x_{in}} - \sum \dot{E}_{x_{out}} = \sum \dot{E}_{x_{dest}} \tag{2.17}$$

The above equation (Eq. 2.17) can be written as;

$$\sum \dot{E}_{x_{heat}} - \sum \dot{E}_{x_{work}} + \sum \dot{E}_{x_{mass,in}} - \sum \dot{E}_{x_{mass,out}} = \sum \dot{E}_{x_{dest}} \tag{2.18}$$

The above equation can be rewritten as:

$$\sum \left(1 - \frac{T_a}{T_{abs}}\right) Q_s - \dot{W} + \dot{m}\left(\psi_{in} - \psi_{out}\right) = \dot{E}_{x_{dest}} \tag{2.19}$$

where

$\dot{Q}_s = I\,(\alpha\tau)\,A_c$ = solar radiant energy rate absorbed by the absorber plate of SAH

$$\psi_{in} = (h_{in} - h_a) - T_a\,(s_{in} - s_a) \tag{2.20}$$

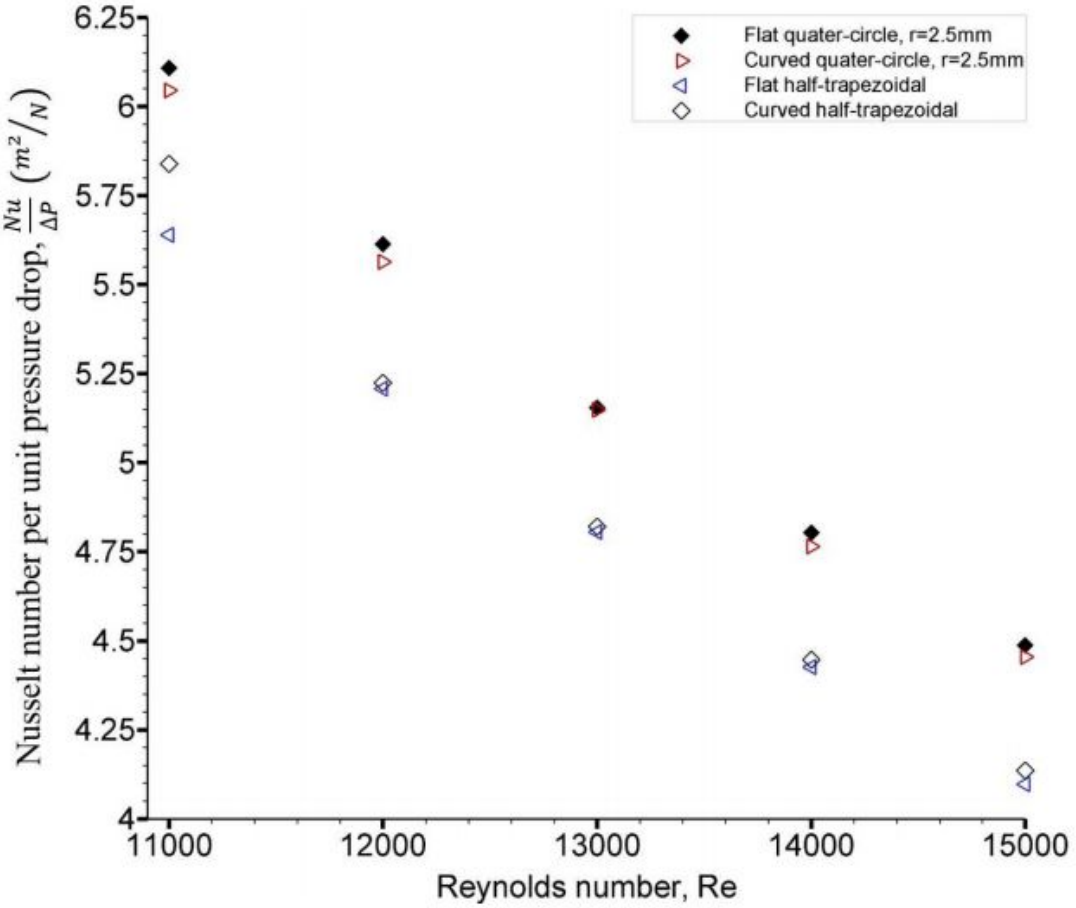

Figure 2.10: Plot $\left(\frac{Nu}{\Delta P}\right)$ vs. Re at $q = 1000\ \mathrm{W/m^2}$ for various shape of ribs.

$$\psi_{out} = (h_{out} - h_a) - T_a\,(s_{out} - s_a) \tag{2.21}$$

The change in entropy and enthalpy of air in the solar air heater are expressed as:

$$\Delta h = (h_{out} - h_{in}) = C_p\,(T_{out} - T_{in}) \tag{2.22}$$

$$\Delta s = (s_{out} - s_{in}) = C_p\,ln\left(\frac{T_{out}}{T_{in}}\right) - R\,ln\left(\frac{P_{out}}{P_{in}}\right) \tag{2.23}$$

$$\left(1 - \frac{T_a}{T_{pm}}\right)\dot{Q}_s - \dot{m}C_p\,(T_{out} - T_{in}) + T_a\,\dot{m}\,(s_{out} - s_{in}) = \dot{E}_{x_{dest}} \tag{2.24}$$

The destruction of exergy or irreversibility (I) represents lost of work i.e. irreversibility can be expressed as follows:

$$\dot{E}_{x_{dest}} = I = T_a\dot{S}_{gen} \tag{2.25}$$

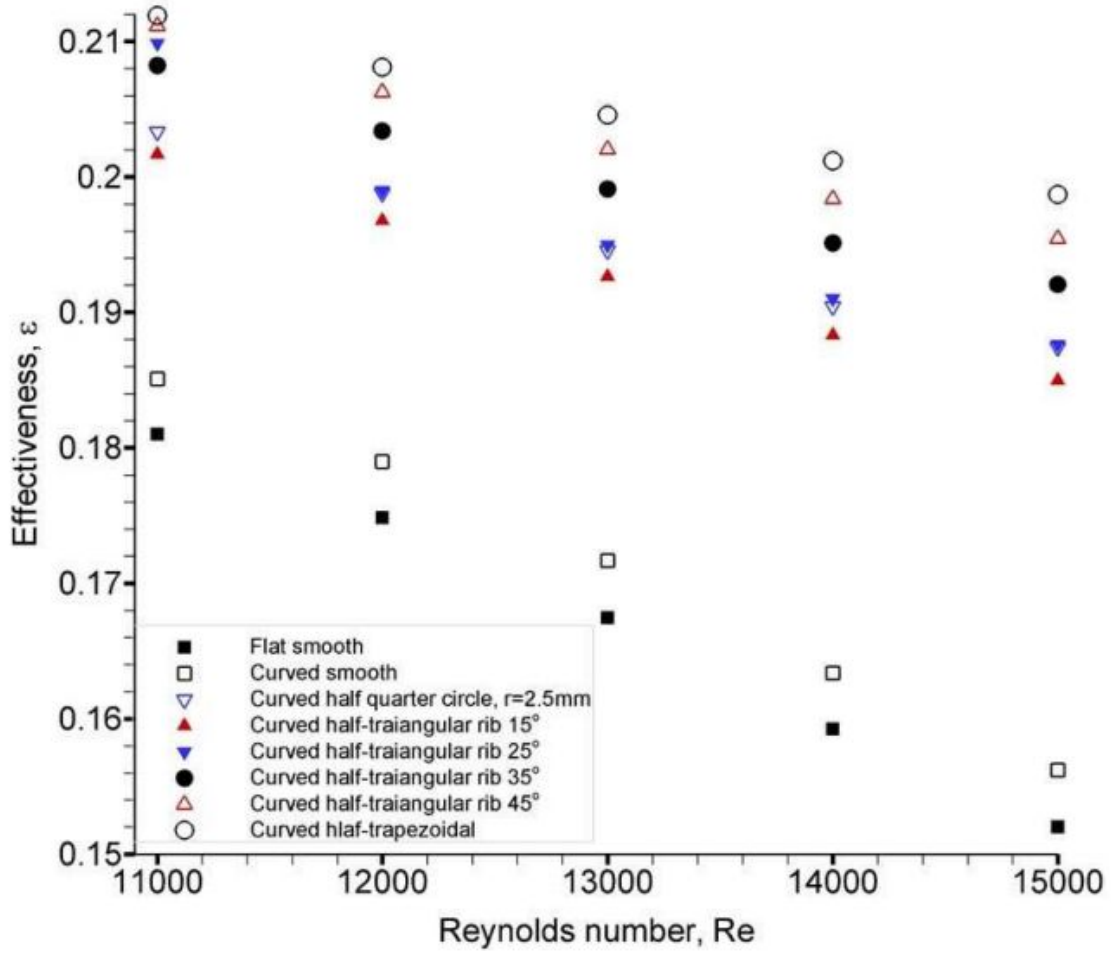

Figure 2.11: Variation of effectiveness of different shape of ribs with *Re*, at $q = 1000\ \mathrm{W/m^2}$.

The exergy efficiency of steady flow solar air heater can be expressed in the form of second law efficiency as:

$$\eta_{II} = \frac{\text{Exergy recovered}}{\text{Exergy supplied}} = \frac{\dot{m}\left[C_p\left(T_{out} - T_{in}\right) - T_a\left(s_{out} - s_{in}\right)\right]}{\left(1 - \frac{T_a}{T_{pm}}\right)\dot{Q}_s} = 1 - \frac{T_a \dot{S}_{gen}}{\left[\left(1 - \frac{T_a}{T_{pm}}\right)\dot{Q}_s\right]} \tag{2.26}$$

The above form of second law efficiency is in the form of first law efficiency, and hence second law efficiency attains maximum value at maximum value of heat flux.

Figure 2.12 shows the exergy recovery of curved and flat- SAH devices with respect to temperature factor of different shape of ribs for the range of *Re* 11000 – 15000, at $q = 1000\ \mathrm{W/m^2}$. The exergy represents the amount of useful energy recovered from the available energy source. The increase in exergy content manifests into decrease in irreversibility of the SAH thereby signifying enhanced thermal performance of the device. The maximum exergy value associated with trapezoidal ribs equipped curved SAH, followed by quarter-circle ribs in comparison to the

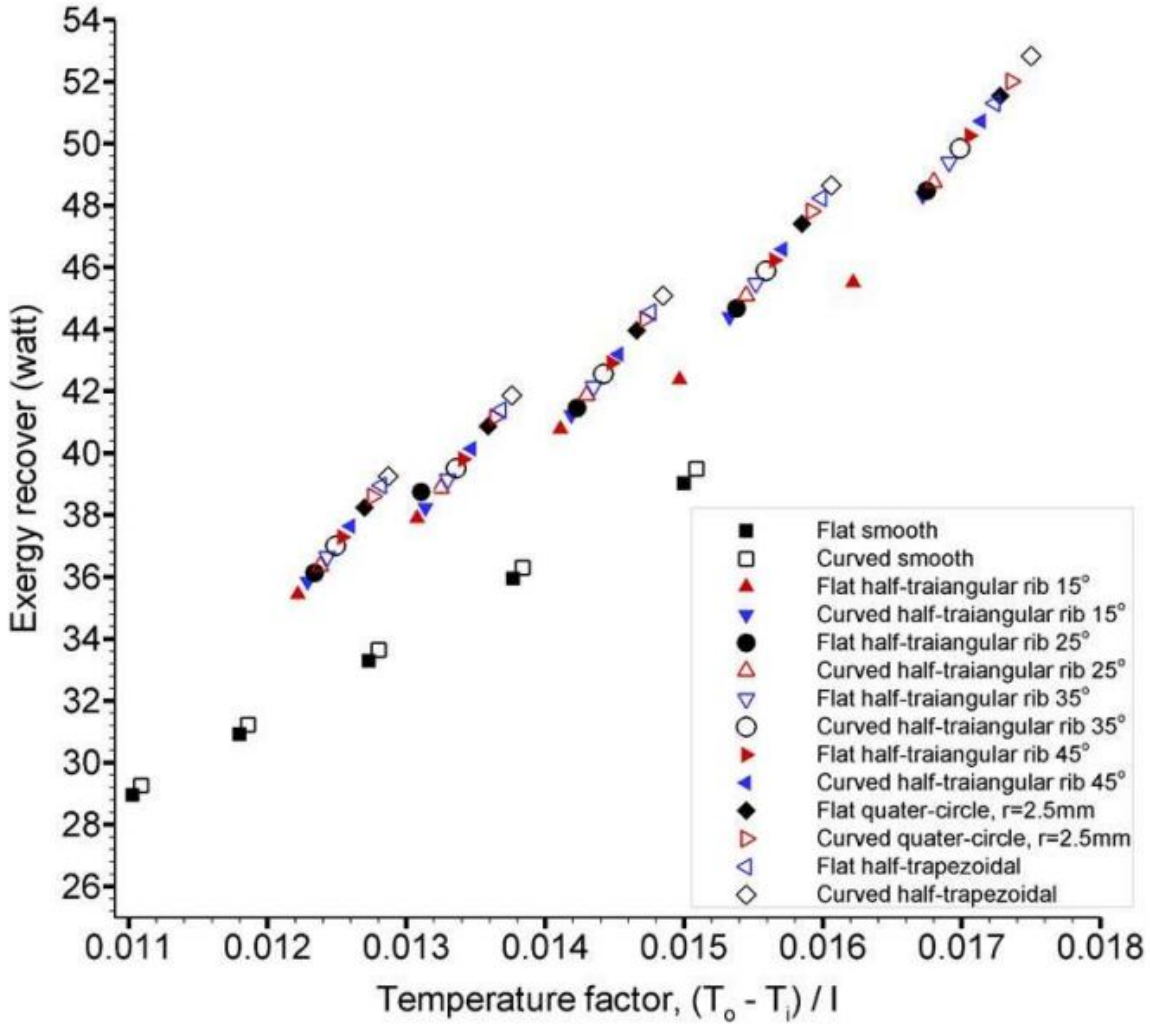

Figure 2.12: Demonstrates variation of exergy recovery of curved and flat- SAH devices with respect to temperature factor of different shape of ribs for the range of *Re* 11000-15000, at $q = 1000\ \mathrm{W/m^2}$.

flat SAH geometry. The same pattern has been followed by the second law efficiency (η_{II}) with maximum values associated with the trapezoidal ribs equipped curved SAH and next highest for quarter-circle ribs as shown in Fig 2.13.

The stagnation region form near the ribs as the flow moves through the flow channel. The friction losses in case of half-trapezoidal ribs are substantially higher in comparison to quarter-circle ribs (see Fig. 2.8), and hence the flow velocity near the absorber plate is little less when compared to quarter-circle ribs. The circular curvature of quarter-circle ribs assist the flow to pass over them with minimum obstructions. In case of half-trapezoidal shape ribs, the inclined edge suddenly becomes flat at the top surface which offers more obstruction resulting in rapid interaction among adjacent fluid layers, which consequently enhances the rate of heat exchange at the expense of higher hydraulic losses.

Figure 2.14 (a), (b) and (c) shows vorticity, turbulent dissipation rate and temperature con-

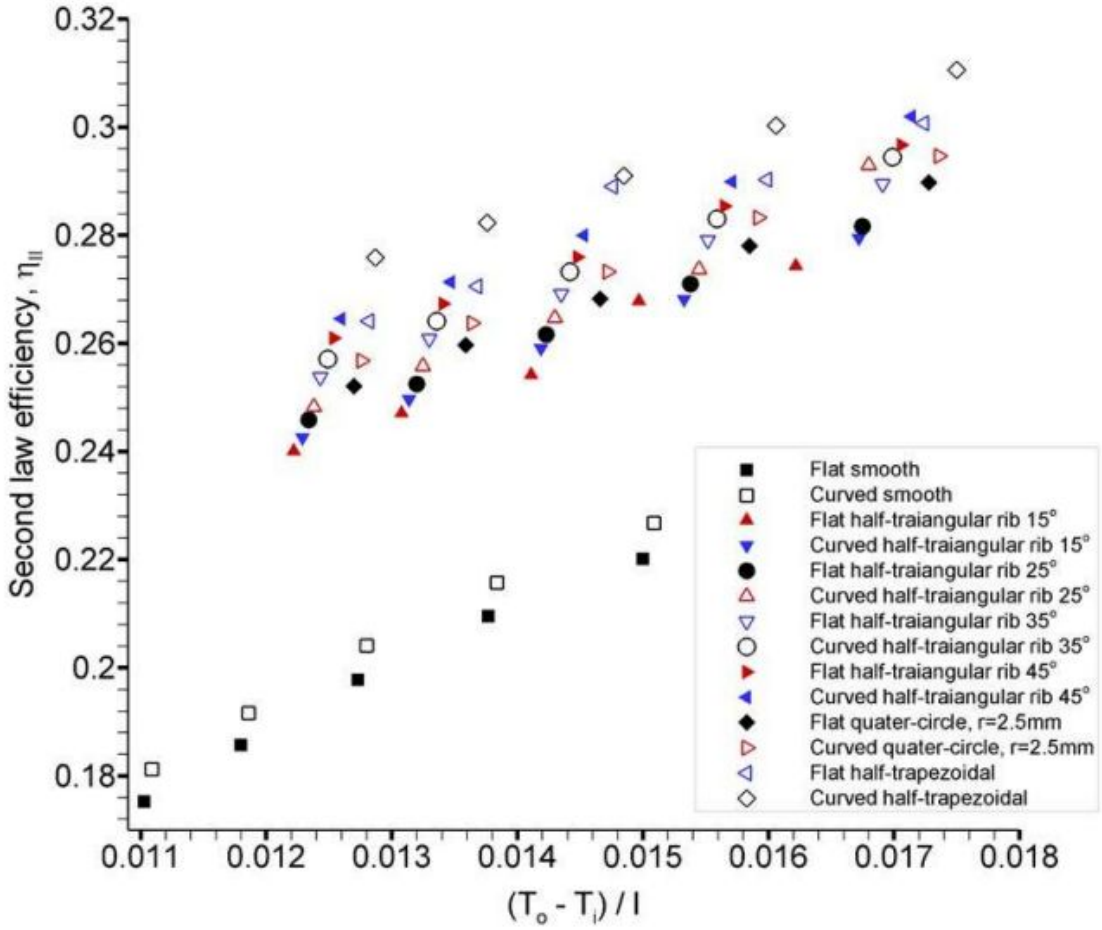

Figure 2.13: Demonstrates second law efficiency (η_{II}) variation of curved and flat- SAH devices with respect to temperature factor of different shape of ribs for the range of *Re* 11000 – 15000, at $q = 1000$ W/m^2.

tours of the curved SAH equipped with e_{tp}/b_{tp}= 1 and quarter-circle ribs having $e_r/H = 0.125$ and e_r/b_r=1, half-trapezoidal ribs having e_{tp}/H= 0.125 and half-triangular ribs having $e_t/H = 0.125$ and e_t/b_t =1, respectively, for the Reynolds number of 11000, at $q = 1000$ W/m^2. The stagnation region form near the ribs as the flow moves through the flow channel. The friction losses in the case of half-trapezoidal ribs are substantially higher in comparison to quarter-circle ribs (see Fig. 2.8), and hence the flow velocity near the absorber plate is little less when compared to quarter-circle ribs. The circular curvature of quarter-circle ribs assists the flow to pass over them with minimum obstructions. In case of half-trapezoidal shape ribs, the inclined edge suddenly becomes flat at the top due to this sharp bend more obstruction offered to flow which enhances mixing in the flow. The enhanced mixing rate increases the heat exchange rate between high-temperature absorber plate and flow adjacent to absorber wall. The hydraulic losses are higher for half-triangular rib shape because of more obstruction offered by sharp-pointed vortex of the triangle.

The thermal performance of the device also varies with the rate of turbulent dissipation. This

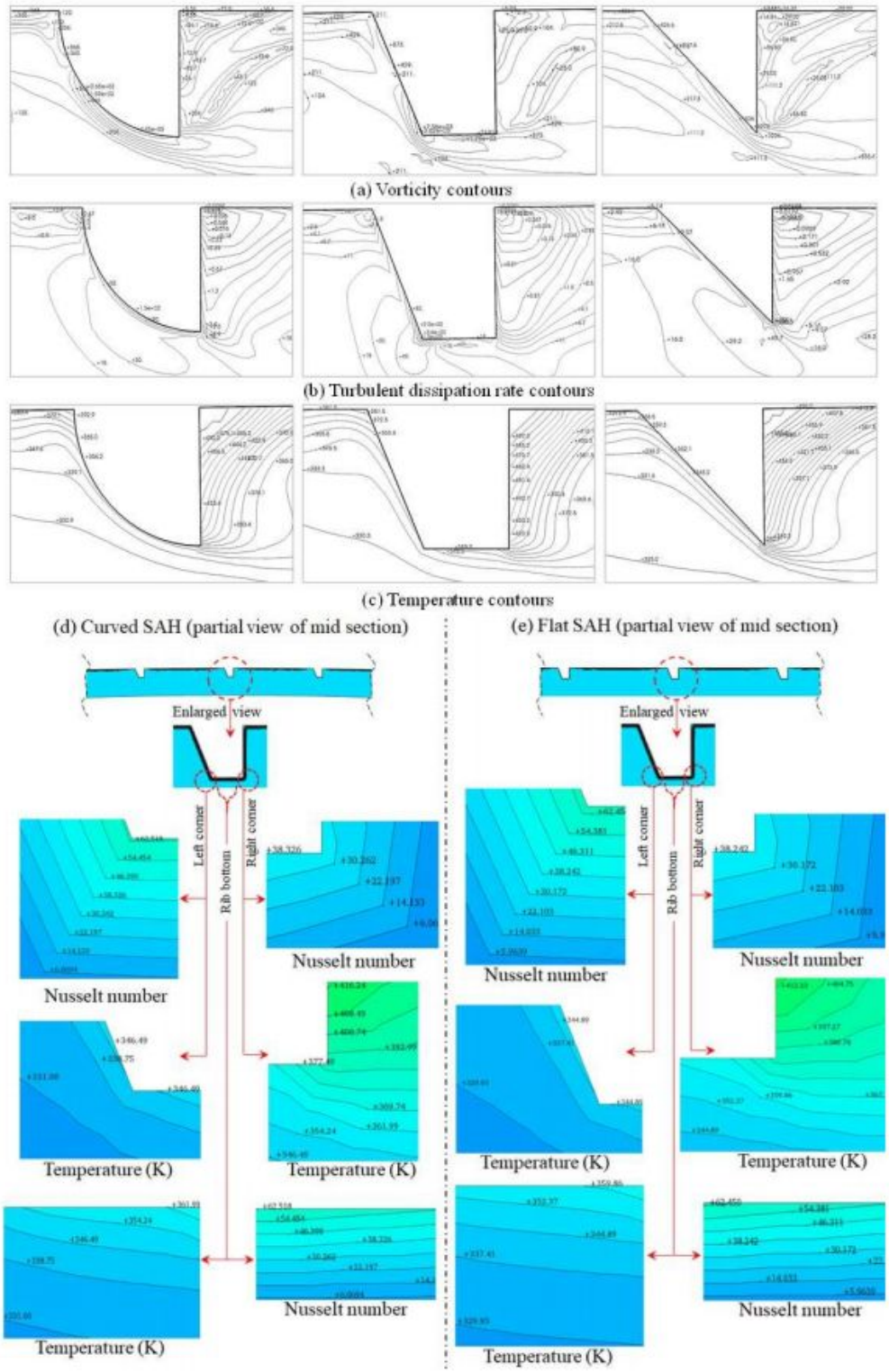

Figure 2.14: (a) Vorticity, (b) turbulent dissipation rate and (c) temperature contours of the curved SAH equipped with quarter-circle ribs having e_r/H = 0.125 and e_r/b_r=1, half-trapezoidal ribs having e_{tp}/H=0.125and half-triangular ribs having e_t/H=0.125ande_t/b_t=1, respectively, for the Reynolds number of 11,000, at q = 1000 W/m^2; (d) and (e) showing the Nusselt number and temperature contours at various regions for the best performing half-trapezoidal ribs at the middle section of curved and flat SAH, respectively.

term describes the rate at which turbulent kinetic energy is dissipated into internal thermal energy. The turbulent kinetic energy signifies the energy accompanied by eddies in the turbulent flows. The results obtained for turbulent dissipation rate have been obtained for all different geometrical shapes of ribs of SAH. The maximum value of turbulent dissipation rate has been observed for half-trapezoidal ribs having $e_{tp}/H = 0.125$ and $e_{tp}/b_{tp} = 1$, whereas next maximum for quarter-circle ribs having $e_r/H = 0.125$ and $e_r/b_r = 1$, and minimum for half-triangular ribs having $e_t/H = 0.125$ and $e_t/b_t = 1$ is shown in Fig. 2.14(b). The more energy associated with the eddies results in higher mixing rate in the flow near absorber vicinity. The enhanced mixing in the flow in a SAH flow channel consequently enhances the rate of heat transfer to fluid medium i.e. air. Fig. 2.14(c) shows temperature contours for various shapes of ribs, among which maximum temperature of the flow has been observed for half-trapezoidal ribs, next maximum for quarter-circle ribs and minimum for half-triangular ribs. The flow separates up to larger distance in between adjacent ribs in case of half-triangular ribs due to sharp edge of triangle tip, and hence major flow portion do not interact with the hot absorber surface is the reason for low thermal performance and higher frictional loss.

For a comparative analysis between curved and flat SAH geometry, the Nusselt number and temperature contours for best performing half-trapezoidal ribs have been shown in the Fig. 2.14 (d) and (e). The Nusselt number of the fluid near the rib surface of curved SAH is higher than the flat plate SAH which represents higher heat transfer rate in case of curved SAH.

Figure 2.15 shows the local Nusselt number variation in best performing half-trapezoidal curved and smooth curved- SAH. The Nusselt numbers for trapezoidal rib are significantly higher compared to smooth flow passage due to increase in the turbulent kinetic energy of the fluid which improved the mixing rate in the flow field. At the inlet maximum temperature gradient between the ambient air and the absorber plate exist and hence maximum Nu value, however Nu value decreases as temperature difference decreases along the flow channel. The Nu value first decreases from 1-2 (see inset) near the leading edge of the rib due to formation of stagnation zone. However, at the bottom of the rib the flow velocity increases from 2-3 which increases Nu value to a maximum level (see point 3 in inset). After the flow separation, primary vortices formed at the right edge of the rib and generation of secondary vortices at the downstream develop adverse pressure gradient which decreases Nu value from 3 to 4 as shown in the inset of Fig. 2.15. Nu values again increases from 4-5 at the downstream due to better mixing in the main stream flow due to flow reattachment.

2.6 Development of Correlations

The thermo-hydraulic performance of curved SAH varies with the Reynolds number, Re and the groove height ratio, e_r/H. The different geometrical ribs have been considered in the present analysis to study the thermal and hydraulic behavior of the solar air heater having curved flow

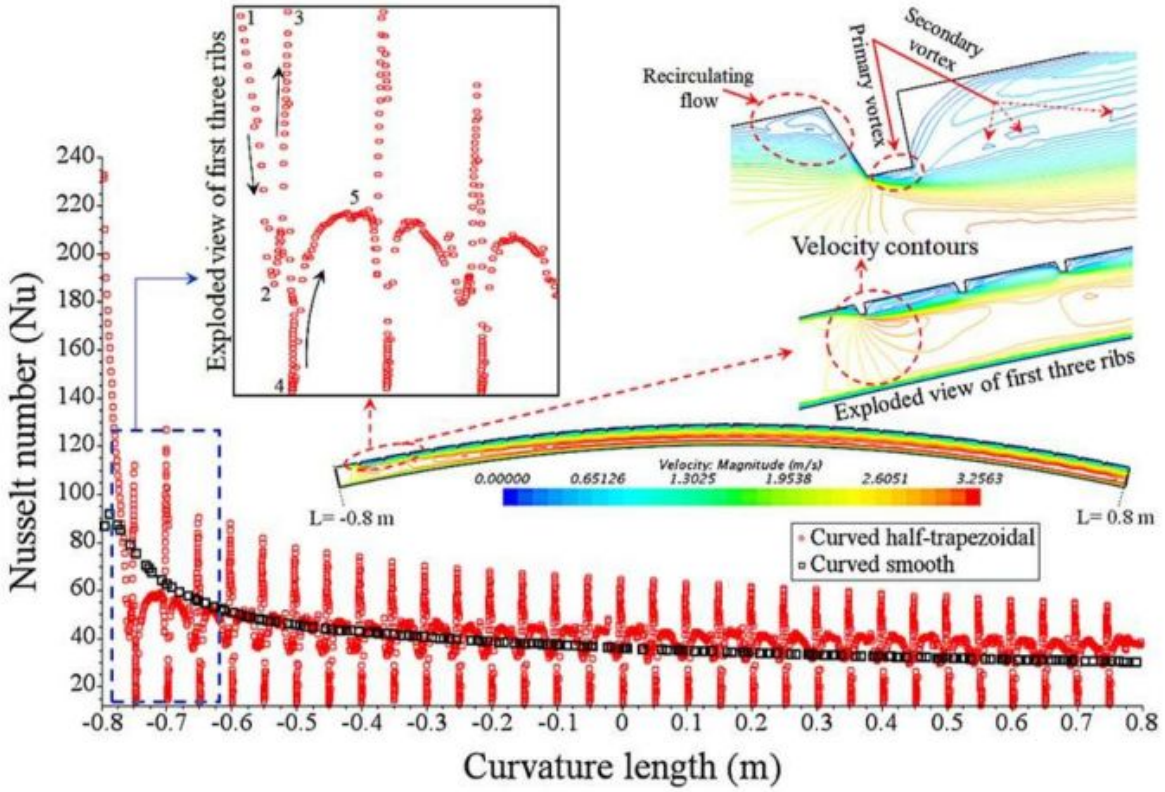

Figure 2.15: Plot of Nusselt number along the absorber length of best performing curved half-trapezoidal ribbed SAH having e_{tp}/H= 0.125 and smooth curved SAH for the Reynolds number 11000, at q = 1000 W/m^2. Magnified views of velocity contours are also shown at different axial locations along the duct height. Notice how Nu continuously decrease in both the cases, however, Nu shoots up at the location of ribs.

passage, among which the quarter-circle ribs offered best thermo-hydraulic performance. An individual correlation has been obtained for best rib design i.e. quarter-circle for curved SAH. The dependent variable i.e. Nusselt number varies with the independent variables is expressed in the form,

$$Nu = f\left[Re, \frac{e_r}{H}\right] \tag{2.27}$$

The final developed correlation has been shown in this section, for intermediate steps refer Apendix A.

The functional relationship among ln(A_o) and ln($\frac{e_r}{H}$) was obtained in the form given in Eq. 2.28. The deviation in the trend among data points is shown in Fig. 2.16;

The expression of Nusselt number, *Nu* obtained using all data points in the final form given below,

$$Nu = B_o\, Re^{0.78}\, ln(e_r/H)^{6.85}\, exp[0.82.ln(e_r/H)^3 + 4.12.ln(e_r/H)^2] \tag{2.28}$$

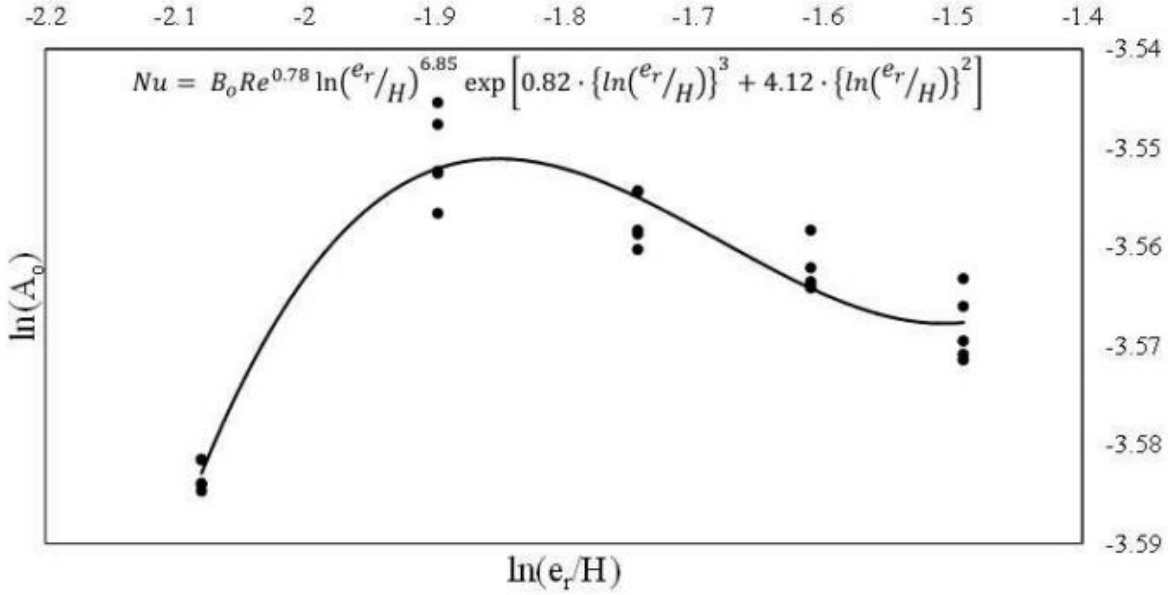

Figure 2.16: Variation of $\ln A_o$ vs. $\ln \frac{e_r}{H}$.

where coefficient $B_o = 1.2$.

Note that the correlation is valid for quarter-circle ribs having relative height ratio, $0.125 \leq \frac{e_r}{H} \leq 0.225$, for constant ribs pitch of 50 mm.

The Nu values obtained using correlations are compared with the numerical values (see Fig. 2.17). The value of mean percentage deviation among the projected data was 0.73%.

2.7 Conclusions

The present study has been performed to determine effective geometrical shape of ribs in down-configuration in a curved SAH device to augment thermo-hydraulic performance. The heat transfer characteristics were obtained for different range of Reynolds number under constant solar insolation condition. The comparisons were made between flat and curved flow passage, respectively for smooth and roughened flow channels of SAH. The following important observations are made:

1. The down-configuration half-trapezoidal and quarter-circle ribs curved SAH show higher thermal performance. The maximum percentage increase in temperature factor was observed for trapezoidal ribs and it was about 17% higher than the conventional flat SAH.

2. The down-configuration quarter-circle ribs offer 10-12% higher thermohydraulic performance i.e. $\frac{(T_o - T_i)}{I} / f$, and Nusselt number per unit pressure drop ($Nu/\Delta P$) in comparison to half trapezoidal ribs. The maximum exergy content was associated with curved SAH integrated with down-configuration ribs of half-trapezoidal and quarter-circle shapes.

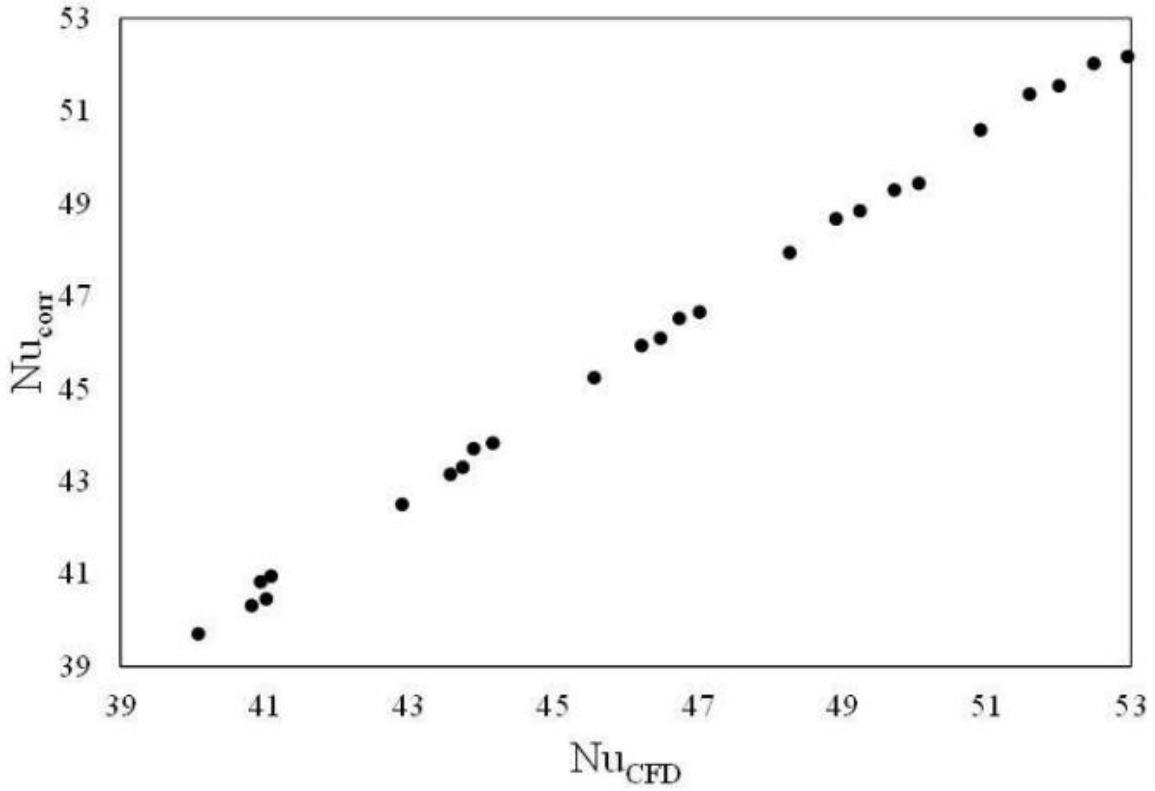

Figure 2.17: Comparison of Nusselt number values obtained numerically and derived correlation.

3. Ribs with quarter-circle shape offer less obstruction to airflow in the flow vicinity of SAH in comparison to half-trapezoidal shape ribs. The friction factor for half trapezoidal ribs was found to be about 10% higher than the quarter-circle ribs, for the range of Reynolds number 11000-15000.

4. A new correlation was developed for Nusselt number variations a function of Reynolds number and geometric parameters for the down-configuration of quarter-circle shapes. The correlation has the form: $Nu = B_o Re^{0.78} \ln\left(\frac{e_r}{H}\right)^{6.85} \exp$, where $B_0 = 1.2$.

The findings of this investigation would be beneficial to researchers in industry and academia in developing effective designs of curved solar air heater that offers higher thermal performance and lower hydrodynamic losses in a wide range of flow parameters and turbulator designs.